Article

Large Low-Field Reversible Magnetocaloric Effect in Itinerant-Electron $Hf_{1-x}Ta_xFe_2$ Alloys

Zhao Song [1], Zongbin Li [1],*[ID], Bo Yang [1], Haile Yan [1], Claude Esling [2], Xiang Zhao [1] and Liang Zuo [1][ID]

[1] Key Laboratory for Anisotropy and Texture of Materials (Ministry of Education), School of Materials Science and Engineering, Northeastern University, Shenyang 110819, China; 15926343131@163.com (Z.S.); yangb@atm.neu.edu.cn (B.Y.); yanhaile@mail.neu.edu.cn (H.Y.); zhaox@mail.neu.edu.cn (X.Z.); lzuo@mail.neu.edu.cn (L.Z.)

[2] Laboratoire d'Étude des Microstructures et de Mécanique des Matériaux (LEM3), CNRS UMR 7239, Université de Lorraine, 57045 Metz, France; claude.esling@univ-lorraine.fr

* Correspondence: lizb@atm.neu.edu.cn

Abstract: First-order isostructural magnetoelastic transition with large magnetization difference and controllable thermal hysteresis are highly desirable in the development of high-performance magnetocaloric materials used for energy-efficient and environmental-friendly magnetic refrigeration. Here, we demonstrate large magnetocaloric effect covering the temperature range from 325 K to 245 K in Laves phase $Hf_{1-x}Ta_xFe_2$ (x = 0.13, 0.14, 0.15, 0.16) alloys undergoing the magnetoelastic transition from antiferromagnetic (AFM) state to ferromagnetic (FM) state on decreasing the temperature. It is shown that with the increase of Ta content, the nature of AFM to FM transition is gradually changed from second-order to first-order. Based on the direct measurements, large reversible adiabatic temperature change (ΔT_{ad}) values of 2.7 K and 3.4 K have been achieved under a low magnetic field change of 1.5 T in the $Hf_{0.85}Ta_{0.15}Fe_2$ and $Hf_{0.84}Ta_{0.16}Fe_2$ alloys with the first-order magnetoelastic transition, respectively. Such remarkable magnetocaloric response is attributed to the rather low thermal hysteresis upon the transition as these two alloys are close to intermediate composition point of second-order transition converting to first-order transition.

Keywords: magnetocaloric effect; magnetic transition; adiabatic temperature change; laves phase

1. Introduction

Magnetic refrigeration, as an alternative cooling technology with the promises of high-efficiency and environment-friendly, has been recognized as a competitive substitute to replace the conventional gas-compression based refrigeration technology. Magnetic refrigeration is designed on the basis of magnetocaloric effect (MCE) [1], which is an intrinsic magneto-thermodynamic property of magnetic materials, using the isothermal magnetic entropy change (ΔS_M) or the adiabatic temperature change (ΔT_{ad}) on exposure to a magnetic field as the performance index. From the viewpoint of practical applications, high-performance magnetocaloric materials, especially those with large reversible MCE actuated at relatively low magnetic field (no more than 2 T), are highly sought in accelerating the commercialization process of magnetic refrigeration. In recent years, the utilization of first-order magnetic transition with large magnetization jump to achieve giant MCE has become the focus of discussion. Several representative alloy systems, such as La-Fe-Si [2–4], Mn-Fe-P-As (Ge, Si) [5–7], Gd-Si-Ge [8,9] and Heusler type Ni-Mn-based alloys [10–15], have been well developed.

In general, the first-order magnetic transition can be categorized into two types [16,17]. One is the magnetostructural transition, where the crystal structure is simultaneously changed in association with the magnetic transition, and the other is the magnetoelastic transition without symmetry breaking. In the case of magnetostructural transition, it is frequently observed that giant magnetocaloric response is achieved for the first application

but significantly weakened for the subsequent field cycling [10], suffering from the large thermal hysteresis rendered by the misfits of two lattices. Such irreversibility in MCE thus raises strong reservations in potential applications. In contrast, for the magnetoelastic transition with the isosymmetric characteristic, the shortcomings relevant to the hysteresis and irreversibility can be effectively manipulated through composition tuning [6].

An interesting system exhibiting the magnetoelastic transition is the itinerant-electron pseudobinary $Hf_{1-x}Ta_xFe_2$ alloys with hexagonal (MgZn$_2$-type) Laves phase structure, experiencing the iso-structural transition from antiferromagnetic (AFM) state to ferromagnetic (FM) state on decreasing the temperature [18–21]. In these alloys, the AFM to FM transition temperature is very sensitive to the Ta content, where increasing Ta content results in considerable decrease in the AFM to FM transition temperature [18]. In contrast, the Néel temperature for the transition from paramagnetic (PM) state to AFM state is less influenced by the content of Ta. For the $Hf_{1-x}Ta_xFe_2$ alloys with $x = 0.125$–0.175, the Néel temperature is located within temperature range from 334 K to 338 K [22]. A detailed phase diagram can be found in the reference [18], where $x = 0.13$ is demonstrated to be close to the critical point for the convergence of AFM, FM and PM states. It is noted that these alloys are known to exhibit the distinct negative thermal expansion behaviors, as the AFM to FM transition is accompanied by the expansion in the lattice [18]. Furthermore, the discontinuity in the magnetization across the AFM to FM transition can also be served as the basis to explore large MCE [20,23,24]. Even though large ΔS_M values have been demonstrated in various alloys [23,24], direct measurements on ΔT_{ad} are still lack. It is worth mentioning that according to the relation $\Delta T_{ad} \approx -T\Delta S_M/C_p$, a lower specific heat capacity C_p is very favorable to achieve higher ΔT_{ad} [25]. Thus, when taking into account the relatively low C_p in the $Hf_{1-x}Ta_xFe_2$ alloys [26], they are very promising candidates to demonstrate considerably large ΔT_{ad} values. Especially, at the borderline of a first-order and a second-order transition [17], a combination of large ΔT_{ad} and good cyclic performance can be expected.

In this work, the magnetocaloric properties in the $Hf_{1-x}Ta_xFe_2$ ($x = 0.13, 0.14, 0.15, 0.16$) alloys were explored. Here, the composition selection was aimed at exploring the MCE in the vicinity of room temperature, based on the phase diagram shown in the literature [18]. Results show that increasing the content of Ta results in the gradual decrease of the AFM to FM transition temperature and also the change of magnetic transition from the second-order to the first-order. For a straightforward evaluation of magnetocaloric properties, the ΔT_{ad} values were directly measured. In the vicinity of the intermediate composition point of second-order transition converting to first-order transition, large reversible ΔT_{ad} values of 2.7 K and 3.4 K have been demonstrated under a low magnetic field change of 1.5 T in the $Hf_{0.85}Ta_{0.15}Fe_2$ alloy and $Hf_{0.84}Ta_{0.16}Fe_2$ alloy, respectively, due to the rather low thermal hysteresis upon the first-order magnetic transition.

2. Materials and Methods

The polycrystalline alloys with the nominal compositions of $Hf_{1-x}Ta_xFe_2$ ($x = 0.13, 0.14, 0.15, 0.16$) were prepared by arc-melting under the protection of high purity argon atmosphere, using the high-purity (4N) metal elements as the raw materials. For achieving a good composition homogeneity, each alloy was melted four times. The as-cast alloys were then encapsulated into vacuumed quartz tubes and isothermally annealed at 1273 K for one week, followed by quenching into water.

The crystal structure analyses were performed by X-ray diffraction (XRD) with Cu-Kα radiation in a Rigaku SmartLab diffractometer (Rigaku, Tokyo, Japan,) equipped with a temperature control attachment. The iso-field ($M(T)$ curves) and iso-thermal ($M(H)$ curves) magnetization measurements were carried out in a Quantum Design MPMS-3 system (Quantum Design, San Diego, CA, USA,), using the disc shaped samples with the dimension of $\Phi 3 \times 1$ mm and the weight of ~0.09 g. To reduce the influence of internal demagnetization field, the magnetic field was applied along circular plane. The specific heat capacity (C_p) was measured by the modulated differential scanning calorimetry (DSC)

technology (TA-DSC 25). Direct measurements of adiabatic temperature change (ΔT_{ad}) induced by magnetic field change were performed in a self-designed experimental device. The temperature range for such device is 223–343 K and the magnetic field, produced by NbFeB permanent magnet in Halbach array, is 1.5 T. Since the magnetic field is stationary, the adiabatic magnetization and demagnetization processes are realized through moving the sample into and out of the uniform magnetic field region, where the sample is placed in a movable rod controlled by servo motor. The time for move-in or move-out is 1 s. Thus, the rate of magnetic field change is 1.5 T s^{-1}. The temperature change of the sample (dimension: $\Phi 10 \times 2$ mm, ~2 g) induced by magnetic field change applied along circular plane was measured by a thermocouple directly attached to the sample surface.

3. Results

Figure 1a shows the powder XRD patterns for the $Hf_{1-x}Ta_xFe_2$ (x = 0.13, 0.14, 0.15, 0.16) alloys measured at the room temperature. It is seen that all the alloys present the characteristic of hexagonal $MgZn_2$-type structure, with the space group of $P6_3/mmc$ (C14 Laves phase). In the lattice, Fe atoms are expected to be located at 2*a* and 6*h* sites and Hf/Ta atoms at 4*f* site [19]. Figure 1b shows the compositional dependence of lattice parameters for the $Hf_{1-x}Ta_xFe_2$ alloys as determined from the XRD patterns. With the increase of Ta content, the lattice parameters *a* and *c* almost linearly decrease. The decrease in lattice parameters *a* and *c* indicates the shrink of lattice volume, which should be attributed to the relatively lower atomic radius of Ta (1.43 Å) with respect to that of Hf (1.56 Å).
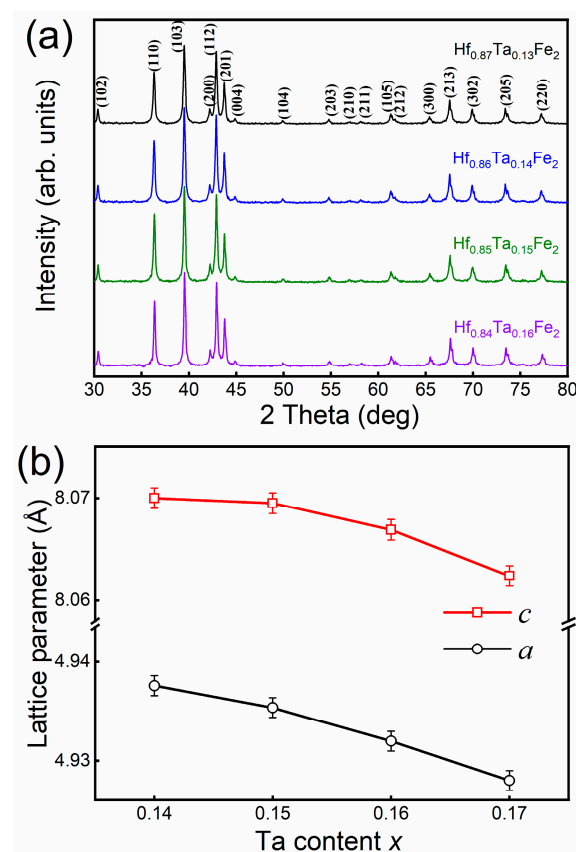

Figure 1. (**a**) Powder X-ray diffraction patterns for the $Hf_{1-x}Ta_xFe_2$ (x = 0.13, 0.14, 0.15, 0.16) alloys; (**b**) Compositional dependence of lattice parameters.

Figure 2a shows the temperature dependence of magnetization (*M*(*T*) curves) under the field of 0.005 T for the $Hf_{1-x}Ta_xFe_2$ alloys. For each alloy, the abrupt change in magnetization on cooling corresponds to the transition from high-temperature AFM phase to low-temperature FM phase. Apparently, the AFM to FM transition temperature (T_t) is

susceptible to the composition variation and T_t gradually decreases as the increase of Ta content. It is noted that for the $Hf_{0.87}Ta_{0.13}Fe_2$, $Hf_{0.86}Ta_{0.14}Fe_2$ and $Hf_{0.85}Ta_{0.15}Fe_2$ alloys, the $M(T)$ branch on cooling is almost overlapped with that on heating, indicating the nature of second-order transition. Accordingly, the T_t temperatures for these three alloys are determined to be 323 K ($Hf_{0.87}Ta_{0.13}Fe_2$), 302 K ($Hf_{0.86}Ta_{0.14}Fe_2$) and 277 K ($Hf_{0.85}Ta_{0.15}Fe_2$), respectively. On the other hand, for the $Hf_{0.84}Ta_{0.16}Fe_2$ alloy, a thermal hysteresis of ~2 K between cooling and heating paths can be observed and the averaged T_t is estimated to be 248 K, suggesting the nature of first-order transition. Nevertheless, such thermal hysteresis remains to be quite low, which is conducive to the reversibility of MCE. Based on the $M(T)$ curves, it is inferred that the increase of Ta content allows a gradual evolution in the nature of magnetic transition from second-order to first-order.
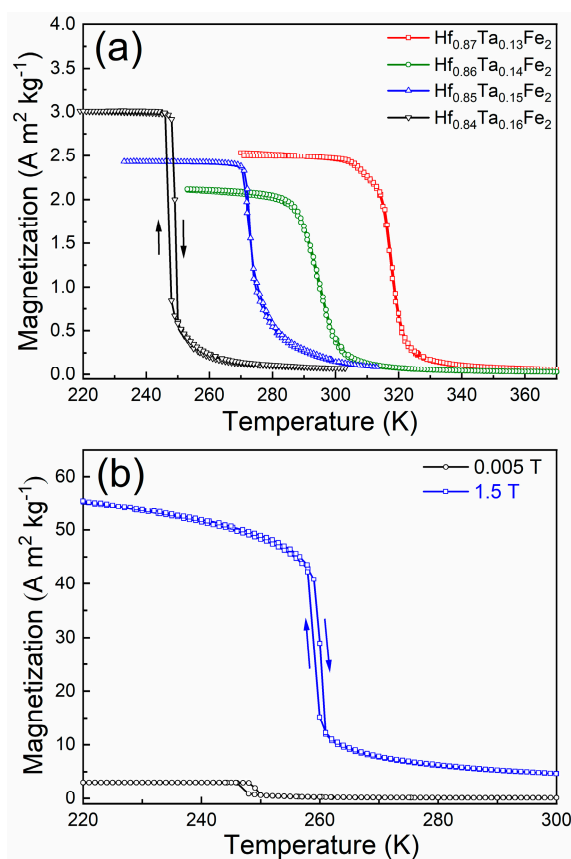

Figure 2. (**a**) Temperature dependence of magnetization ($M(T)$ curves) under the field of 0.005 T for the $Hf_{1-x}Ta_xFe_2$ (x = 0.13, 0.14, 0.15, 0.16) alloys. (**b**) Comparison on the $M(T)$ curves under 0.005 T and 1.5 T for the $Hf_{0.84}Ta_{0.16}Fe_2$ alloy.

Figure 2b compares the $M(T)$ curves under the field of 0.005 T and 1.5 T for the $Hf_{0.84}Ta_{0.16}Fe_2$ alloy. It is evidenced that the AFM to FM transition is accompanied by large magnetization jump. Owing to such magnetization difference, the AFM to FM transition is thus shifted to higher temperature region on increasing the magnetic field, since the magnetic field favors the phase with high magnetization. Under the field of 1.5 T, the AFM to FM transition temperature can be increased by 11 K, with the rate of 7.3 K T^{-1}.

To acquire further insights into the magnetic transition for the $Hf_{1-x}Ta_xFe_2$ alloys, field-up and field-down isothermal magnetization ($M(H)$) curves across the AFM to FM transition were measured with the maximum field up to 5 T, as shown in Figure 3. The $M(H)$ curves were measured in a discontinuous protocol. Prior to the measurements at each temperature, the sample was firstly zero field heated to a temperature well above the AFM to FM transition temperature, and then zero field cooled down to the measuring temperature. After that, the field-up and field-down $M(H)$ curves were measured. For

the $Hf_{0.87}Ta_{0.13}Fe_2$ alloy (Figure 3a), typical ferromagnetic behavior can be observed at the temperatures below T_t (i.e., 323 K), where the magnitude of saturation magnetization gradually increases with decreasing the temperature. At the temperatures above 323 K, the field dependence of magnetization tends to exhibit a linear relation, showing the typical characteristic of antiferromagnetic state. It is noted that there is no obvious magnetic hysteresis between field-up and field-down $M(H)$ curves. The $M(H)$ curves for the $Hf_{0.86}Ta_{0.14}Fe_2$ alloy exhibit similar characteristics with those of $Hf_{0.87}Ta_{0.13}Fe_2$ alloy, as demonstrated in Figure 3b.
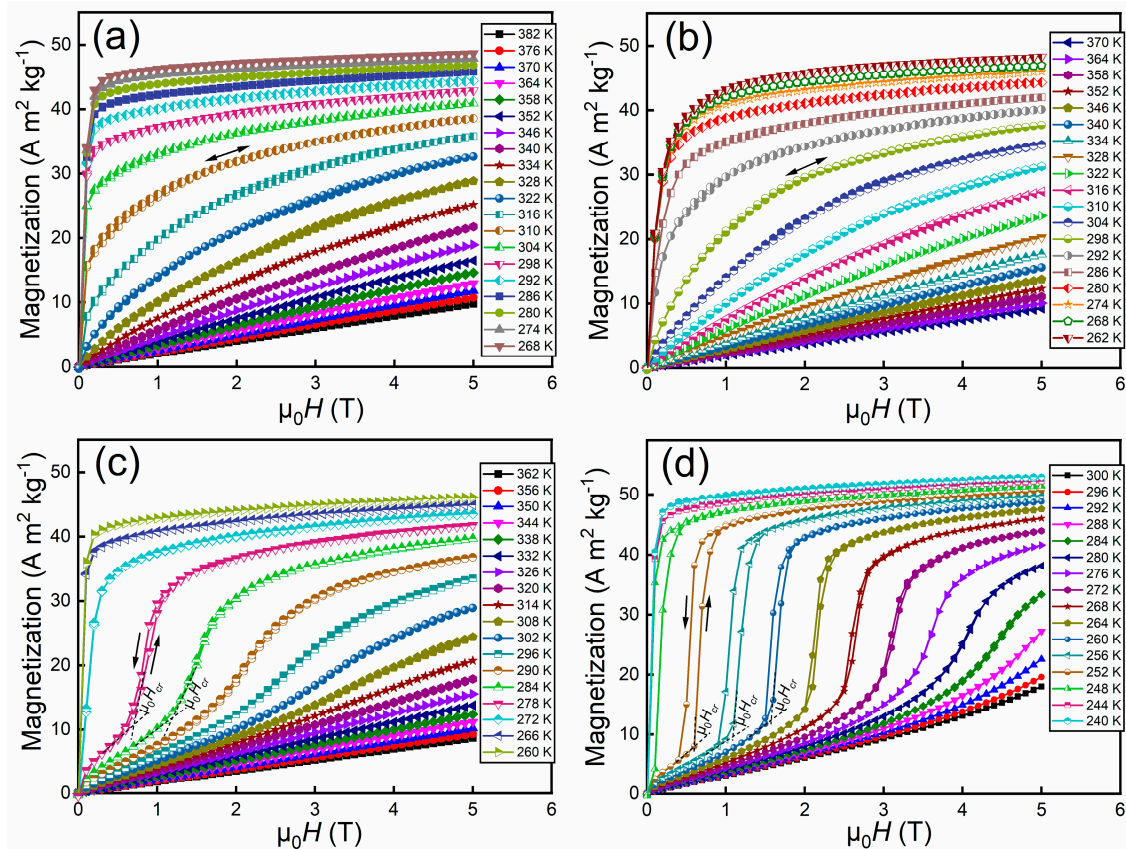

Figure 3. Field-up and field-down isothermal $M(H)$ curves for the $Hf_{1-x}Ta_xFe_2$ alloys. (**a**) $Hf_{0.87}Ta_{0.13}Fe_2$; (**b**) $Hf_{0.86}Ta_{0.14}Fe_2$; (**c**) $Hf_{0.85}Ta_{0.15}Fe_2$; (**d**) $Hf_{0.84}Ta_{0.16}Fe_2$.

In the case of $Hf_{0.85}Ta_{0.15}Fe_2$ alloy (Figure 3c), the $M(H)$ curves exhibit the typical characteristic of ferromagnetism with no obvious magnetic hysteresis at the temperatures below T_t (i.e., 277 K). Above 277 K, step-like magnetization behavior can be observed, where a sudden jump in the slope followed by a rapid increase in magnetization at a certain critical field $\mu_0 H_{cr}$ takes place. This phenomenon is an indication of magnetic field-induced metamagnetic transition from AFM state to FM state. It is noted that magnetic field-induced AFM to FM transition is fully reversible, with very low magnetic hysteresis (e.g., ~0.1 T at 278 K) between the field-up and field-down isothermal magnetization curves. In addition, the critical field $\mu_0 H_{cr}$ to drive the AFM to FM transition is gradually elevated as the increase of temperature. As for the $M(H)$ curves of $Hf_{0.84}Ta_{0.16}Fe_2$ alloy demonstrated in Figure 3d, sharp step-like magnetization behaviors can be observed above T_t, indicating the occurrence of metamagnetic transition. Even though the magnetic hysteresis is widened when compared to that of $Hf_{0.85}Ta_{0.15}Fe_2$ alloy, it remains in a relatively low level, e.g., ~0.2 T at 252 K.

In order to verify the nature of magnetic transition for the $Hf_{1-x}Ta_xFe_2$ alloys, the Arrott plots were calculated by using the field-up isothermal magnetization curves [27],

as shown in Figure 4. Since there is no negative slope for the Arrott plots in Figure 4a,b, the magnetic transition for the $Hf_{0.87}Ta_{0.13}Fe_2$ alloy and the $Hf_{0.86}Ta_{0.14}Fe_2$ alloy can be confirmed to be second-order. In contrast, the typical *S*-shape of Arrott plots manifests the first-order nature of magnetic transition for the $Hf_{0.85}Ta_{0.15}Fe_2$ alloy (Figure 4c) and the $Hf_{0.84}Ta_{0.16}Fe_2$ alloy (Figure 4d). Thus, the change of second-order transition to first-order transition appears at a tricritical point, which should lay somewhere at the composition $x = 0.14–0.15$.

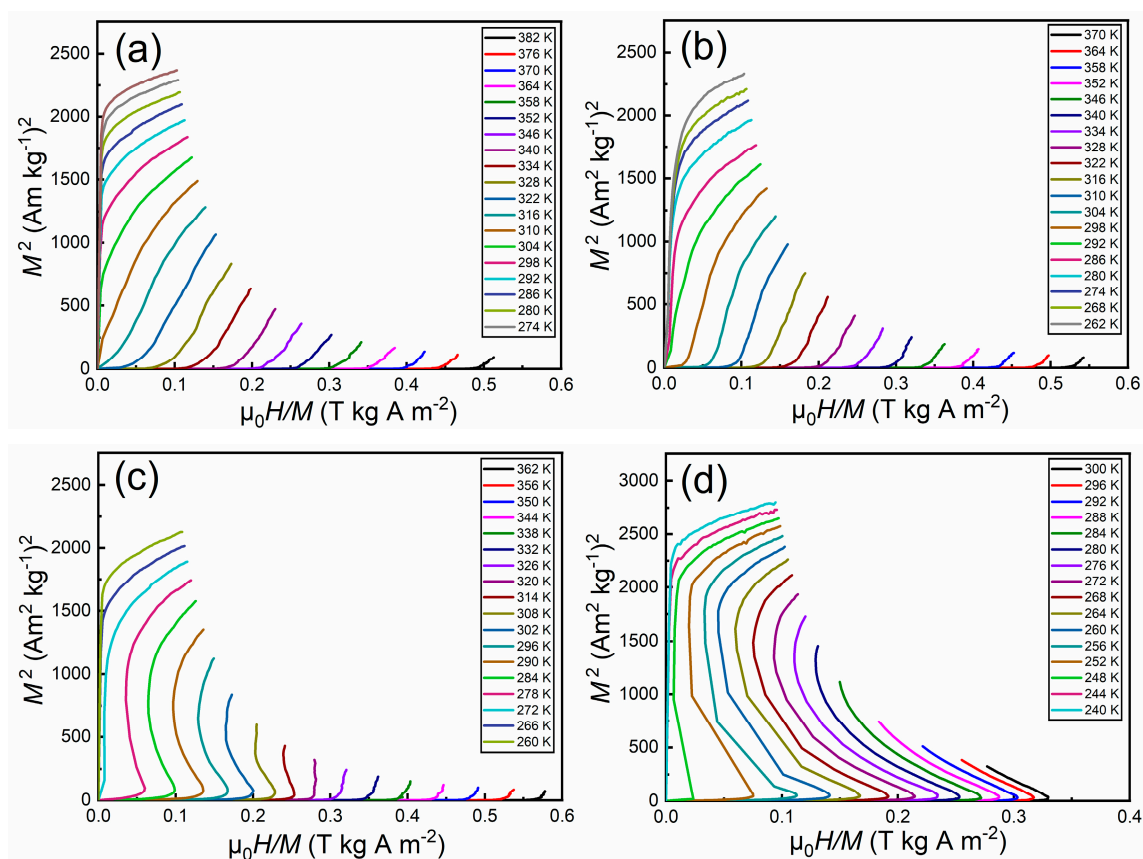**Figure 4.** Arrott plots for the $Hf_{1-x}Ta_xFe_2$ alloys. (**a**) $Hf_{0.87}Ta_{0.13}Fe_2$; (**b**) $Hf_{0.86}Ta_{0.14}Fe_2$; (**c**) $Hf_{0.85}Ta_{0.15}Fe_2$; (**d**) $Hf_{0.84}Ta_{0.16}Fe_2$.

As the $Hf_{0.84}Ta_{0.16}Fe_2$ alloy exhibits a sharp first-order magnetoelastic transition, temperature dependent XRD measurements were performed in order to acquire deep insights into the crystal structure evolution concomitant with the magnetoelastic transition. Figure 5a shows the temperature dependent XRD patterns for the $Hf_{0.84}Ta_{0.16}Fe_2$ alloy across the first-order AFM-FM transition. It is seen that the hexagonal symmetry for the $Hf_{0.84}Ta_{0.16}Fe_2$ alloy remains unchanged upon the magnetic transition, confirming the characteristic of a magnetoelastic transition. Figure 5b plots the change of lattice parameters *a* and *c* as a function of temperature. On decreasing the temperature, the lattice constant *c* exhibits a gradual decrease in the measured temperature region, i.e., positive thermal expansion. In contrast, a sharp increase in the lattice constant *a* can be observed upon the occurrence of AFM-FM transition, with the ratio $\Delta a/a$ of 0.26%, showing the characteristic of negative thermal expansion. It is noted that the obvious discontinuity in the lattice parameter *a* is a reflection of first-order magnetoelastic transition. Figure 5c shows the temperature dependence of unit cell volume. It is evidenced that the magnetoelastic transition is accompanied by the increase in the unit cell volume and the volume change $\Delta V/V$ is estimated to be 0.51%. Such negative thermal expansion should be attributed to the large discontinuity in the lattice parameter *a*.
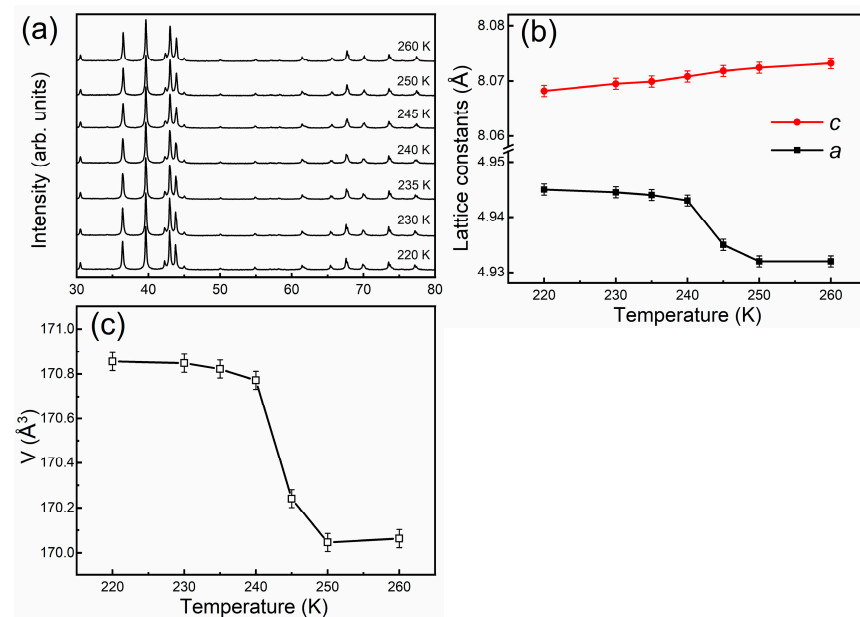
Figure 5. (**a**) Temperature dependent XRD patterns for the $Hf_{0.84}Ta_{0.16}Fe_2$ alloy; (**b**) Change of lattice parameters *a* and *c* as a function of temperature; (**c**) Temperature dependence of unit cell volume.

Based on the field-up $M(H)$ curves, the magnetic field induced entropy change ΔS_M was calculated by using the Maxwell relation [1]. Under the field change of 1.5 T, the ΔS_M values of -1.72 J kg^{-1} K^{-1}, -1.77 J kg^{-1} K^{-1}, -3.04 J kg^{-1} K^{-1} and -5.21 J kg^{-1} K^{-1} can be obtained for the $Hf_{0.87}Ta_{0.13}Fe_2$, $Hf_{0.86}Ta_{0.14}Fe_2$, $Hf_{0.85}Ta_{0.15}Fe_2$ and $Hf_{0.84}Ta_{0.16}Fe_2$ alloys, respectively, as demonstrated in Figure 6. In addition, under the field change of 5 T, the corresponding ΔS_M values are -4.0 J kg^{-1} K^{-1} ($Hf_{0.87}Ta_{0.13}Fe_2$), -4.17 J kg^{-1} K^{-1} ($Hf_{0.86}Ta_{0.14}Fe_2$), -4.97 J kg^{-1} K^{-1} ($Hf_{0.85}Ta_{0.15}Fe_2$) and -6.26 J kg^{-1} K^{-1} ($Hf_{0.84}Ta_{0.16}Fe_2$). With the evolution of magnetic transition from second-order to first-order, the maximum ΔS_M values are gradually increased. Moreover, the refrigerant capacity (*RC*) for the present alloys was also determined based on the ΔS_M values [1]. The *RC* values under the field change of 5 T are 135 J kg^{-1}, 131 J kg^{-1}, 126 J kg^{-1} and 173 J kg^{-1} for the $Hf_{0.87}Ta_{0.13}Fe_2$, $Hf_{0.86}Ta_{0.14}Fe_2$, $Hf_{0.85}Ta_{0.15}Fe_2$ and $Hf_{0.84}Ta_{0.16}Fe_2$ alloys, respectively.

It has been reported that the order of magnetic transition can also be quantitatively analyzed by calculating the power law exponent *n* based on the ΔS_M values [17], i.e., $n = d\ln|\Delta S_M|/d\ln H$. In the temperature range of magnetic transition, $n > 2$ represents the first-order transition, whereas $n < 2$ indicates the second-order transition. The temperature dependence of the exponent *n* for the present alloys under the field of 1.5 T was also calculated and presented in Figure 6. For the $Hf_{0.87}Ta_{0.13}Fe_2$ and $Hf_{0.86}Ta_{0.14}Fe_2$ alloys, the exponent *n* exhibits a trend of 1→minimum→2, evidencing the second-order transition [17]. For the $Hf_{0.85}Ta_{0.15}Fe_2$ and $Hf_{0.84}Ta_{0.16}Fe_2$ alloys, the magnitude of exponent *n* higher than 2 clearly demonstrates the first-order transition [17]. The determination of magnetic transition order by the exponent *n* is consistent with the results obtained by the Arrott plots.

Adiabatic temperature change (ΔT_{ad}), as an important performance index of MCE, allows a straightforward assessment on the magnetocaloric properties [1]. Here, the ΔT_{ad} values for the studied $Hf_{1-x}Ta_xFe_2$ alloys under a low field change of 1.5 T were directly measured under the discontinuous protocol. Figure 7a shows the temperature dependence of ΔT_{ad} values on cooling for the studied $Hf_{1-x}Ta_xFe_2$ alloys on applying the magnetic field of 1.5 T. For the $Hf_{0.87}Ta_{0.13}Fe_2$ and $Hf_{0.86}Ta_{0.14}Fe_2$ alloys with the second-order magnetic transition, the temperature evolution of ΔT_{ad} values is moderate and gradual, covering a wide temperature range. Under the field change $\mu_0\Delta H$ of 1.5 T, the maximum ΔT_{ad} values of 1.4 K and 1.7 K can be obtained around the AFM-FM transition for the $Hf_{0.87}Ta_{0.13}Fe_2$ and $Hf_{0.86}Ta_{0.14}Fe_2$ alloys, respectively. The temperature dependence of ΔT_{ad} values for the $Hf_{0.85}Ta_{0.15}Fe_2$ and $Hf_{0.84}Ta_{0.16}Fe_2$ alloys with the first-order magnetic transition is

sharp and abrupt, appearing in a relatively narrow temperature range. Accordingly, the maximum ΔT_{ad} values up to 2.7 K and 3.4 K can be achieved in the $Hf_{0.85}Ta_{0.15}Fe_2$ and $Hf_{0.84}Ta_{0.16}Fe_2$ alloys, respectively. It is shown that the height and width of the ΔT_{ad} curves for the $Hf_{1-x}Ta_xFe_2$ alloys are in agreement with the first-order and second-order nature of the magnetic transitions. With the change of magnetic transition from second-order to first-order, the maximum ΔT_{ad} values are also gradually enhanced, in line with the evolution of ΔS_M values. It should be mentioned that although the ΔS_M values obtained in the present alloys are not very remarkable, the ΔT_{ad} values are quite impressive, especially for the alloys with the first-order magnetic transition. This effect could be due to the relatively low specific heat capacity C_p for the $Hf_{1-x}Ta_xFe_2$ alloys (e.g., $C_p = {\sim}300$ J kg^{-1} K^{-1} for the $Hf_{0.84}Ta_{0.16}Fe_2$ alloy, as shown in inset of Figure 7a), according to the relation $\Delta T_{ad} \approx -T\Delta S_M/C_p$. By using the C_p and the ΔS_M value at 252 K (i.e., -5.21 J kg^{-1} K^{-1}) for the $Hf_{0.84}Ta_{0.16}Fe_2$ alloy, the maximum ΔT_{ad} value can be estimated to be 4.4 K under a magnetic field change $\mu_0\Delta H$ of 1.5 T, being relatively higher than that obtained by direct measurements.
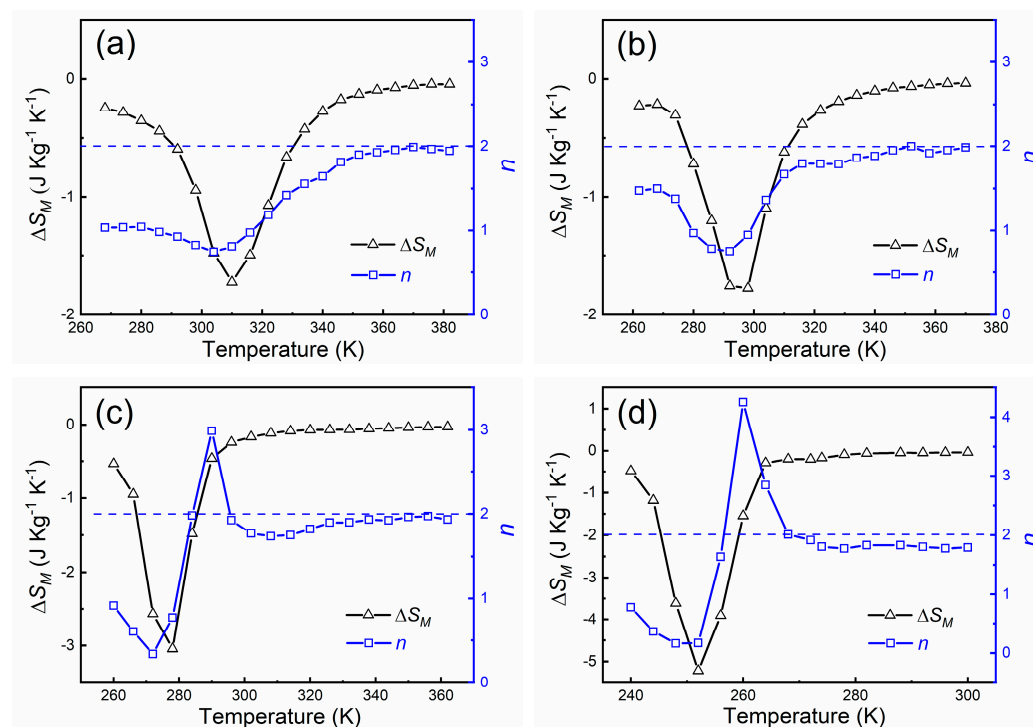

Figure 6. Temperature dependence of ΔS_M and exponent n at the field of 1.5 T for the $Hf_{1-x}Ta_xFe_2$ alloys. (**a**) $Hf_{0.87}Ta_{0.13}Fe_2$; (**b**) $Hf_{0.86}Ta_{0.14}Fe_2$; (**c**) $Hf_{0.85}Ta_{0.15}Fe_2$; (**d**) $Hf_{0.84}Ta_{0.16}Fe_2$.

The reversibility of ΔT_{ad} for the magnetocaloric materials is of great importance for the potential applications. Considering the characteristic of zero hysteresis for the second-order magnetic transition, ΔT_{ad} values for the $Hf_{0.87}Ta_{0.13}Fe_2$ and $Hf_{0.86}Ta_{0.14}Fe_2$ alloys are fully reversible. For the $Hf_{0.85}Ta_{0.15}Fe_2$ and $Hf_{0.84}Ta_{0.16}Fe_2$ alloys with the first-order magnetic transition, they also present very good reversibility in the ΔT_{ad} values during the cyclic magnetization/demagnetization measurements. Figure 7b,c show the reversible behavior of ΔT_{ad} values for the $Hf_{0.85}Ta_{0.15}Fe_2$ at 275 K and the $Hf_{0.84}Ta_{0.16}Fe_2$ alloys at 253 K under the field change of 1.5 T, respectively. The $Hf_{1-x}Ta_xFe_2$ alloys exhibit conventional MCE due to the transition from AFM state to FM state on cooling. Thus, the sample warms on magnetization and cools on demagnetization. Stable reversible ΔT_{ad} value of 2.7 K for the $Hf_{0.85}Ta_{0.15}Fe_2$ alloy and 3.4 K for the $Hf_{0.84}Ta_{0.16}Fe_2$ alloy can be achieved during the cyclic magnetization/demagnetization measurements. Such good reversibility should be attributed to that the rather low thermal hysteresis upon the magnetic transition, since these two alloys lay at the borderline of the first-order transition and the second-order

transition. Table 1 compares the present reversible ΔT_{ad} values with those for some typical magnetocaloric materials. The present reversible ΔT_{ad} values are superior to those obtained in some alloys with magnetostructural transition.
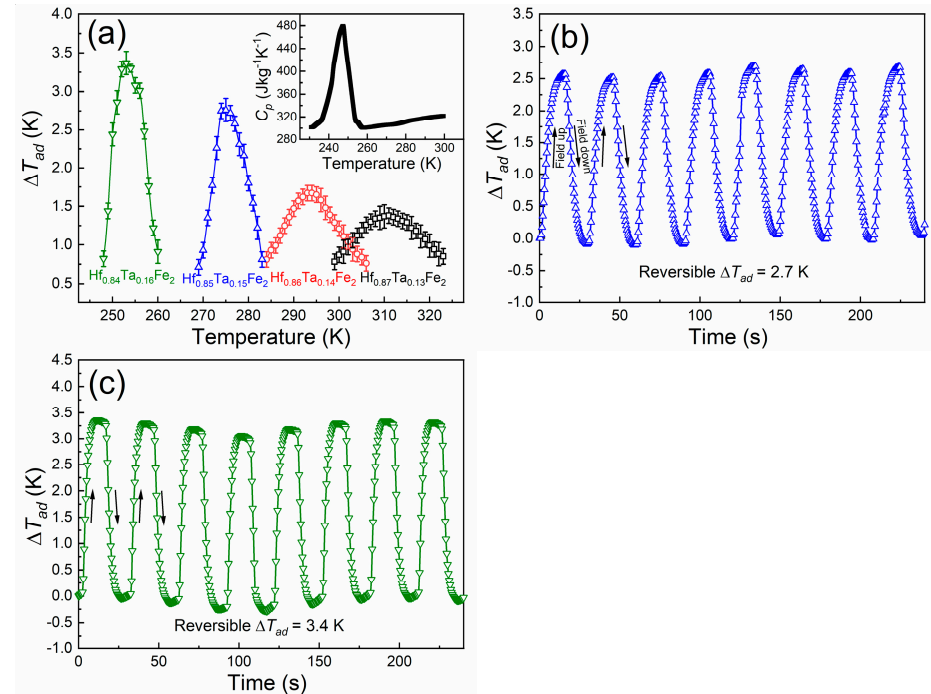

Figure 7. (**a**) Directly measured temperature dependence of ΔT_{ad} curve for $Hf_{1-x}Ta_xFe_2$ (x = 0.13, 0.14, 0.15, 0.16) alloys under the field change of 1.5 T. The inset shows the specific heat capacity for the $Hf_{0.84}Ta_{0.16}Fe_2$ alloy. The cyclic adiabatic temperature change for (**b**) $Hf_{0.85}Ta_{0.15}Fe_2$ alloy at 275 K and (**c**) $Hf_{0.84}Ta_{0.16}Fe_2$ alloy at 253 K.

Table 1. Comparisons on the maximum reversible adiabatic temperature changes of some typical magnetocaloric materials reported in the literatures.

Alloys	Transition Type	Temperature (K)	ΔT_{cyclic}^{max} (K)	$\mu_0\Delta H$ (T)	Reference
$Hf_{0.85}Ta_{0.15}Fe_2$	Magnetoelastic	275	2.7	1.5	This work
$Hf_{0.84}Ta_{0.16}Fe_2$	Magnetoelastic	253	3.4	1.5	This work
$MnFe_{0.95}P_{0.595}B_{0.075}Si_{0.33}$	Magnetoelastic	277	2.8	1.1	[6]
$Fe_{49}Rh_{51}$	Magnetoelastic	321	6.2	1.9	[28]
Eu_2In	Magnetoelastic	56	5.0	2.0	[16]
$Mn_{1.87}Cr_{0.13}Sb_{0.95}Ga_{0.05}$	Magnetoelastic	280	1.9	5.0	[29]
Mn_3GaC	Magnetoelastic	150	3.0	3.0	[30]
$MnCo_{0.93}Cu_{0.07}Ge$	Magnetostructural	304	1.1	1.1	[31]
$Ni_{40}Co_8Mn_{42}Sn_{10}$	Magnetostructural	298	0.8	1.5	[32]
$Ni_{45.3}Co_{5.1}Mn_{36.1}In_{13.5}$	Magnetostructural	294	1.1	1.5	[33]
$Ni_{46}Co_3Mn_{35}Cu_2In_{14}$	Magnetostructural	272	2.5	1.5	[34]
$Ni_{50}Mn_{35}In_{15}$	Magnetostructural	286	1.5	1.9	[35]
$Ni_{45.7}Mn_{37.9}Sn_{11.8}Co_{4.9}$	Magnetostructural	330	1.2	1.93	[36]
$Ni_{45.7}Mn_{36.6}In_{13.5}Co_{4.2}$	Magnetostructural	282	3.0	1.95	[37]
$Ni_{51.3}Mn_{32.9}In_{15.8}$	Magnetostructural	251	0.7	3.0	[38]

4. Conclusions

In summary, the magnetoelastic transition and the related magnetocaloric effect in Laves phase $Hf_{1-x}Ta_xFe_2$ (x = 0.13, 0.14, 0.15, 0.16) alloys were investigated. It is shown that the increase of Ta content enables the gradual decrease of the AFM to FM transition temperature and also the conversion from the second-order transition to the first-order transition. Owing to the magnetization difference associated with such AFM to FM transition, the MCE is observed in these compounds in the temperature range from 325 K to 245 K. Under a low magnetic field change of 1.5 T, large ΔS_M values of -3.04 J kg^{-1} K^{-1} and -5.21 J kg^{-1} K^{-1} are obtained in the $Hf_{0.85}Ta_{0.15}Fe_2$ and $Hf_{0.84}Ta_{0.16}Fe_2$ alloys with the first-order magnetic transition. Moreover, large reversible ΔT_{ad} values up 2.7 K and 3.4 K are also achieved under a low magnetic field change of 1.5 T in the $Hf_{0.85}Ta_{0.15}Fe_2$ and $Hf_{0.84}Ta_{0.16}Fe_2$ alloys, respectively, being much higher than those obtained in some alloys with magnetostructural transition. Such remarkable magnetocaloric properties should be attributed to the rather low thermal hysteresis of first-order magnetic transition in the $Hf_{0.85}Ta_{0.15}Fe_2$ and $Hf_{0.84}Ta_{0.16}Fe_2$ alloys, as they lay at the borderline of the first-order and the second-order magnetic transition. Furthermore, the effect of doping elements will be explored in the following work towards tuning the magnetization difference across the magnetic transition and the resultant magnetocaloric properties.

Author Contributions: Conceptualization, Z.S. and Z.L.; validation, B.Y. and H.Y.; investigation, Z.S.; writing—original draft preparation, Z.S.; writing—review and editing, Z.L., C.E., X.Z. and L.Z, supervision, C.E.; project administration, X.Z.; funding acquisition, L.Z. All authors have read and agreed to the published version of the manuscript.

Data Availability Statement: The data presented in this study are available on request from the corresponding author.

Conflicts of Interest: The authors declare no conflict of interest.

References

1. Franco, V.; Blázquez, J.S.; Ipus, J.J.; Law, J.Y.; Moreno-Ramírez, L.M.; Conde, A. Magnetocaloric effect: From materials research to refrigeration devices. *Prog. Mater. Sci.* **2018**, *93*, 112–232. [CrossRef]
2. Hu, F.X.; Shen, B.G.; Sun, J.R.; Cheng, Z.H.; Zhang, X.X. Influence of negative lattice expansion and metamagnetic transition on magnetic entropy change in the compound $LaFe_{11.4}Si_{1.6}$. *Appl. Phys. Lett.* **2001**, *78*, 3675–3677. [CrossRef]
3. Fujita, A.; Fujieda, S.; Hasegawa, Y.; Fukamichi, K. Itinerant-electron metamagnetic transition and large magnetocaloric effects in $La(Fe_xSi_{1-x})_{13}$ compounds and their hydrides. *Phys. Rev. B* **2003**, *67*, 104416. [CrossRef]
4. Liu, J.; Krautz, M.; Skokov, K.; Woodcock, T.G.; Gutfleisch, O. Systematic study of the microstructure, entropy change and adiabatic temperature change in optimized La-Fe-Si alloys. *Acta Mater.* **2011**, *59*, 3602–3611. [CrossRef]
5. Tegus, O.; Brück, E.; Buschow, K.H.J.; de Boer, F.R. Transition-metal based magnetic refrigerants for room-temperature applications. *Nature* **2002**, *415*, 150–152. [CrossRef] [PubMed]
6. Guillou, F.; Porcari, G.; Yibole, H.; van Dijk, N.; Brück, E. Taming the first order transition in giant magnetocaloric materials. *Adv. Mater.* **2014**, *26*, 2671–2675. [CrossRef] [PubMed]
7. Trung, N.T.; Ou, Z.Q.; Gortenmulder, T.J.; Tegus, O.; Buschow, K.H.J.; Bruck, E. Tunable thermal hysteresis in MnFe(P, Ge) compounds. *Appl. Phys. Lett.* **2009**, *94*, 102513. [CrossRef]
8. Pecharsky, V.K.; Gschneidner, K.A., Jr. Giant magnetocaloric effect in $Gd_5(Si_2Ge_2)$. *Phys. Rev. Lett.* **1997**, *78*, 4494–4497. [CrossRef]
9. Giguere, A.; Foldeaki, M.; Gopal, B.R.; Chahine, R.; Bose, T.K.; Frydman, A. Direct measurement of the "giant" adiabatic temperature change in $Gd_5Si_2Ge_2$. *Phys. Rev. Let.* **1999**, *83*, 2262–2265. [CrossRef]
10. Liu, J.; Gottschall, T.; Skokov, K.P.; Moore, J.D.; Gutfleisch, O. Giant magnetocaloric effect driven by structural transitions. *Nat. Mater.* **2012**, *11*, 620–626. [CrossRef]
11. Li, Z.B.; Zhang, Y.D.; Sanchez-Valdes, C.F.; Sanchez Llamazares, J.L.; Esling, C.; Zhao, X.; Zuo, L. Giant magnetocaloric effect in melt-spun Ni-Mn-Ga ribbons with magneto-multistructural transformation. *Appl. Phys. Lett.* **2014**, *104*, 044101. [CrossRef]
12. Li, Z.B.; Dong, S.Y.; Li, Z.Z.; Yang, B.; Liu, F.; Sánchez-Valdés, C.F.; Sánchez Llamazares, J.L.; Zhang, Y.D.; Esling, C.; Zhao, X.; et al. Giant low-field magnetocaloric effect in Si alloyed Ni-Co-Mn-In alloys. *Scr. Mater.* **2019**, *159*, 113–118. [CrossRef]

13. Li, Z.B.; Jiang, Y.W.; Li, Z.Z.; Sánchez-Valdés, C.F.; Sánchez Llamazares, J.L.; Yang, B.; Zhang, Y.D.; Esling, C.; Zhao, X.; Zuo, L. Phase transition and magnetocaloric properties of Mn$_{50}$Ni$_{42-x}$Co$_x$Sn$_8$ ($0 \leq x \leq 10$) melt-spun ribbons. *IUCrJ* **2018**, *5*, 54–66. [CrossRef] [PubMed]

14. Koshkid'ko, Y.; Pandey, S.; Cwik, J.; Dubenko, I.; Aryal, A.; Granovsky, A.; Szymanski, D.; Stadler, S.; Lähderanta, E.; Ali, N. Relaxation phenomena in adiabatic temperature changes near magnetostructural transitions in Heusler alloys. *J. Alloys Compd.* **2020**, *821*, 153402. [CrossRef]

15. Koshkid'ko, Y.; Pandey, S.; Quetz, A.; Aryal, A.; Dubenko, I.; Cwik, J.; Dilmieva, E.; Granovsky, A.; Lähderanta, E.; Stadler, S.; et al. Kinetic effects in magnetic and magnetocaloric properties of metamagnetic Ni$_{50}$Mn$_{35}$In$_{14.25}$B$_{0.75}$ alloy. *J. Magn. Magn. Mater.* **2018**, *459*, 98–101. [CrossRef]

16. Guillou, F.; Pathak, A.K.; Paudyal, D.; Mudryk, Y.; Wilhelm, F.; Rogalev, A.; Pecharsky, V.K. Non-hysteretic first-order phase transition with large latent heat and giant low-field magnetocaloric effect. *Nat. Commun.* **2018**, *9*, 2925. [CrossRef]

17. Law, J.Y.; Franco, V.; Moreno-Ramírez, L.M.; Conde, A.; Karpenkov, D.Y.; Radulov, I.; Skokov, K.P.; Gutfleisch, O. A quantitative criterion for determining the order of magnetic phase transitions using the magnetocaloric effect. *Nat. Commun.* **2018**, *9*, 2680. [CrossRef]

18. Li, L.F.; Tong, P.; Zou, Y.M.; Tong, W.; Jiang, W.B.; Jiang, Y.; Zhang, X.K.; Lin, J.C.; Wang, M.; Yang, C.; et al. Good comprehensive performance of Laves phase Hf$_{1-x}$Ta$_x$Fe$_2$ as negative thermal expansion materials. *Acta Mater.* **2018**, *161*, 258–265. [CrossRef]

19. Li, B.; Luo, X.H.; Wang, H.; Ren, W.J.; Yano, S.; Wang, C.W.; Gardner, J.S.; Liss, K.D.; Miao, P.; Lee, S.H.; et al. Colossal negative thermal expansion induced by magnetic phase competition on frustrated lattices in Laves phase compound (Hf,Ta)Fe$_2$. *Phys. Rev. B.* **2016**, *93*, 224405. [CrossRef]

20. Diop, L.V.B.; Kastil, J.; Isnard, O.; Arnol, Z.; Kamarad, J. Magnetic and magnetocaloric properties of itinerant-electron system Hf$_{1-x}$Ta$_x$Fe$_2$ (x = 0.125 and 0.175). *J. Alloys Compd.* **2015**, *627*, 446–450. [CrossRef]

21. Diop, L.V.B.; Isnard, O.; Amara, M.; Gay, F.; Itié, J.P. Giant negative thermal expansion across the first-order magnetoelastic transition in Hf$_{0.86}$Ta$_{0.14}$Fe$_2$. *J. Alloys Compd.* **2020**, *845*, 156310. [CrossRef]

22. Diop, L.V.B.; Kastil, J.; Isnard, O.; Arnold, Z.; Kamarad, J. Collapse of ferromagnetism in itinerant-electron system: A magnetic, transport properties, and high pressure study of (Hf,Ta)Fe$_2$ compounds. *J. Appl. Phys.* **2014**, *116*, 163907. [CrossRef]

23. Li, S.; Yang, J.C.; Zhao, N.; Wang, Q.; Fan, X.M.; Yin, X.W.; Cui, W.B. Phase-transition-induced magneto-elastic coupling and negative thermal expansion in (Hf,Ta)Fe$_{1.98}$ Laves phase. *J. Magn. Magn. Mater.* **2021**, *517*, 167236. [CrossRef]

24. Han, Z.D.; Wang, D.H.; Huang, S.L.; Su, Z.H.; Tang, S.L.; Du, Y.W. Low-field magnetic entropy changes in Hf$_{1-X}$Ta$_X$Fe$_2$. *J. Alloys Compd.* **2004**, *377*, 75–77. [CrossRef]

25. Gottschall, T.; Skokov, K.P.; Fries, M.; Taubel, A.; Radulov, I.; Scheibel, F.; Benke, D.; Riegg, S.; Gutfleisch, O. Making a Cool Choice: The Materials Library of Magnetic Refrigeration. *Adv. Energy Mater.* **2019**, *9*, 1901322. [CrossRef]

26. Bag, P.; Rawat, R.; Chaddah, P.; Babu, P.D.; Siruguri, V. Unconventional thermal effects across first-order magnetic transition in the Ta-doped HfFe$_2$ intermetallic. *Phys. Rev. B* **2016**, *93*, 014416. [CrossRef]

27. Arrott, A. Criterion for ferromagnetism from observations of magnetic isotherms. *Phys. Rev.* **1957**, *108*, 1394–1396. [CrossRef]

28. Chirkova, A.; Skokov, K.P.; Schultz, L.; Baranov, N.V.; Gutfleisch, O.; Woodcock, T.G. Giant adiabatic temperature change in FeRh alloys evidenced by direct measurements under cyclic conditions. *Acta Mater.* **2016**, *106*, 15–21. [CrossRef]

29. Tekgül, A.; Acet, M.; Scheibel, F.; Farle, M.; Ünal, N. The reversibility of the inverse magnetocaloric effect in Mn$_{2-x}$Cr$_x$Sb$_{0.95}$Ga$_{0.05}$. *Acta Mater.* **2017**, *124*, 93–99. [CrossRef]

30. Çakır, Ö.; Acet, M. Reversibility in the inverse magnetocaloric effect in Mn$_3$GaC studied by direct adiabatic temperature-change measurements. *Appl. Phys. Lett.* **2012**, *100*, 202404. [CrossRef]

31. Liu, J.; You, Y.; Batashev, I.; Gong, Y.; You, X.; Huang, B.; Zhang, F.; Miao, X.; Xu, F.; van Dijk, N.; et al. Design of Reversible Low-Field Magnetocaloric Effect at Room Temperature in Hexagonal MnMX Ferromagnets. *Phys. Rev. Appl.* **2020**, *13*, 054003. [CrossRef]

32. Li, Z.B.; Li, Z.Z.; Yang, J.J.; Yang, B.; Zhao, X.; Zuo, L. Large room temperature adiabatic temperature variation in a Ni$_{40}$Co$_8$Mn$_{42}$Sn$_{10}$ polycrystalline alloy. *Intermetallics* **2018**, *100*, 57–62. [CrossRef]

33. Li, Z.Z.; Li, Z.B.; Yang, B.; Zhao, X.; Zuo, L. Giant low-field magnetocaloric effect in a textured Ni$_{45.3}$Co$_{5.1}$Mn$_{36.1}$In$_{13.5}$ alloy. *Scr. Mater.* **2018**, *151*, 61–65. [CrossRef]

34. Li, Z.B.; Yang, J.J.; Li, D.; Li, Z.Z.; Yang, B.; Yan, H.L.; Sánchez-Valdés, C.F.; Llamazares, J.L.S.; Zhang, Y.D.; Esling, C.; et al. Tuning the Reversible Magnetocaloric Effect in Ni–Mn–In-Based Alloys through Co and Cu Co-Doping. *Adv. Electron. Mater.* **2019**, *5*, 1800845. [CrossRef]

35. Gottschall, T.; Skokov, K.P.; Scheibel, F.; Acet, M.; Ghorbani Zavareh, M.; Skourski, Y.; Wosnitza, J.; Farle, M.; Gutfleisch, O. Dynamical Effects of the Martensitic Transition in Magnetocaloric Heusler Alloys from Direct ΔT_{ad} Measurements under Different Magnetic-Field-Sweep Rates. *Phys. Rev. Appl.* **2016**, *2*, 024013. [CrossRef]

36. Taubel, A.; Gottschall, T.; Fries, M.; Riegg, S.; Soon, C.; Skokov, K.P.; Gutfleisch, O. A Comparative Study on the Magnetocaloric Properties of Ni-Mn-X(-Co) Heusler Alloys. *Phy. Status Solidi B* **2018**, *255*, 1700331. [CrossRef]

37. Gottschall, T.; Skokov, K.P.; Frincu, B.; Gutfleisch, O. Large reversible magnetocaloric effect in Ni-Mn-In-Co. *Appl. Phys. Lett.* **2015**, *106*, 021901. [CrossRef]

38. Titov, I.; Acet, M.; Farle, M.; González-Alonso, D.; Mañosa, L.; Planes, A.; Krenke, T. Hysteresis effects in the inverse magnetocaloric effect in martensitic Ni-Mn-In and Ni-Mn-Sn. *J. Appl. Phys.* **2012**, *112*, 073914. [CrossRef]